

1 Rupture Passing Probabilities at Fault Bends and Steps, With Application to
2 Rupture Length Probabilities For Earthquake Early Warning

3
4
5 Glenn P. Biasi¹
6 gbiasi@usgs.gov

7 Steven G. Wesnousky²
8 wesnousky@unr.edu

9
10 ¹ U.S. Geological Survey, 525 S. Wilson Avenue, Pasadena, CA 91106

11 ² Center for Neotectonic Studies and Seismological Laboratory, University of Nevada,
12 Reno, NV 89557, USA.

13
14
15 Keywords. Earthquake Hazards, California,
16
17
18

19 Abstract

20 Earthquake early warning (EEW) systems can quickly identify the onset of an earthquake
21 rupture, but the first few seconds of seismic data only weakly predict the final rupture
22 length. We present two approaches for estimating the conditional probabilities of rupture
23 length given a nucleation point from an EEW system. Bends and steps in a fault are
24 geometric complexities with some probability of arresting rupture. Their effects compound
25 serially with rupture length, and provide a physical basis for probabilistic estimates of where
26 rupture may stop. Applied to a discretized fault model for California, geologically
27 reasonable probabilities of length are found. For an example rupture initiated on the central
28 San Jacinto fault (SJF) 70 km SE of the intersection with the San Andreas fault (SAF), 78%
29 grow to M 6.3, 8% become $M \sim 7.1$ and reach the connection to the SAF, and less than 1%
30 reach 300 km and M 7.7 or larger. For the same nucleation point on the SJF, conditional
31 probabilities of length calculated from Uniform California Earthquake Rupture Forecast v3
32 (UCERF3) rupture rates predict 18% would reach the San Andreas fault, and about 13% will
33 reach 300 km or larger. From geometric complexity, most ruptures on the SAF starting at
34 Bombay Beach in the southern Salton Trough are arrested in the complex Mill Creek
35 section, and only $\sim 5\%$ reach to San Bernardino and become an acute hazard to Los Angeles.
36 Conditional probabilities of length can be precompiled and are of potential use to EEW both
37 for alert planning and operations.

38 Introduction

39 Earthquake early warning (EEW) systems are designed to warn of pending strong shaking
40 from a large earthquake by exploiting the speed advantage of electronically transmitted signals
41 over seismic waves (Cooper, 1868; Heaton, 1985; Kanamori et al., 1997). Efforts to develop,
42 formalize, and apply, EEW methodologies in California have moved forward in concert with
43 advances in seismic instrumentation, telemetry, computers, data storage, and real-time
44 seismological analysis (Chung et al., 2019; Cochran et al., 2019, Kohler et al., 2018; Allen and
45 Kanamori, 2003; Allen et al., 2009; Heaton, 1985; Kanamori et al., 1997; Kanamori et al., 1999;
46 Kanamori, 2005; Wu and Teng, 2002). Methodologies generally entail the rapid estimation of the
47 magnitude of an earthquake from observations of peak displacement, velocity, and acceleration
48 (Wu and Kanamori, 2005; Wu et al., 2007; Wu and Kanamori, 2008) or the predominant period

49 and frequency content (Allen and Kanamori, 2003; Kanamori, 2005; Nakamura, 1988) of the
50 first seconds of the first recorded P-wave.

51 The actual moment released in the first seconds of a large earthquake normally corresponds
52 to an M 6 to 6.5 earthquake. Early work suggested that the eventual magnitude of an earthquake
53 that continues to grow could be known from how it starts (Olson and Allen, 2005). Later studies
54 have questioned this conclusion, and find instead that reliable estimates of final magnitude
55 require more data, from extended P-wave displacements (Yamada and Ide, 2008; Noda and
56 Ellsworth, 2016), up to half or more of the rupture itself (Meier et al., 2016; Trugman et al.,
57 2019). To estimate magnitude and rupture extent of larger earthquakes, the ShakeAlert system
58 includes an algorithm named FinDER (Bose et al., 2012). FinDER estimates event size based on
59 a finite fault model of rupture and ground motion template matching to observed ground
60 motions. The alternative Propagation of Undamped Motion algorithm (PLUM, Kodera, 2018)
61 avoids magnitude estimation altogether and instead predicts alert areas from locations of
62 observed strong ground motions and a forward model of ground motion for growth of the alert
63 area. Originally developed in Japan, PLUM is under evaluation for the ShakeAlert system
64 (Cochran et al., 2019).

65
66 In this paper we present a probabilistic approach for estimating the eventual length of a
67 growing earthquake rupture given the starting location and knowledge of the fault structure.
68 Probabilities conditioned on alert location can be computed in advance for all discrete elements
69 in the fault system. We also develop an alternative approach to integrate the Uniform California
70 Earthquake Rupture Forecast version 3 (UCERF3; Field et al., 2014; Field et al., 2017) into
71 EEW. A priori estimates of rupture length cannot take the place of direct measurement of the
72 rupture under way, but may be useful, for example, to inform policies for alert area as a function
73 of initial earthquake magnitude and location.

74 Estimating Probable Length of Future Earthquakes

75 Discretized Fault Model

76 On a long-term basis, a fault-based rupture forecast such as UCERF3 in California can be
77 used to estimate of the likelihood that a rupture of a given length will occur. However, once a

78 rupture has started, the a priori probabilities of earthquake occurrence no longer apply, and the
 79 length estimate becomes conditional on the starting location and the fault structure connected to
 80 it.

81 To introduce our approach to estimating the probability of eventual rupture length
 82 conditioned on knowledge of initial location, we begin with a simplified discrete fault model
 83 (**Figure 1**). Each subsection models an area nominally ruptured by the time an EEW point
 84 source algorithm could alert and identify that a rupture is under way and could grow. The fault
 85 consists of 9 subsections, and we assume that rupture initiates in the middle, as rupture of panel
 86 S_0 . Given rupture initiation in S_0 and the 9-element discrete model shown, there are 24 possible
 87 rupture extensions (**Figure 1**). If all rupture extents are equally likely (i.e. $p_1=p_2=p_3$ etc.), then
 88 by total probability one may simply count the ruptures with the extent of interest as a fraction of
 89 all possibilities. For example, ruptures 1-4 have unilateral rupture to the right (*ur*) of panel S_0 , so
 90 $P_{ur} = \sum_{i=1}^4 p_i$ Unilateral rupture to the left (*ul*) of panel S_0 is $P_{ul} = \sum_{i=5}^8 p_i$, and the probability
 91 of a bilateral rupture (*bl*) is $P_{bl} = \sum_{i=9}^{24} p_i$. Other cases such as starting in S_0 and ending in panel
 92 S_3 (either bilateral or unilateral) follow by summing the probabilities of the individual ruptures.
 93 Thus, in this simplest model where all ruptures are equally likely, given a rupture initiates in S_0 ,
 94 one may simply count the ruptures involving each of the other subsections (**Figure 2a**) and
 95 translate to probabilities by dividing by the total number of ruptures (bar heights, **Figure 2b**).

96 Modifying the Discretized Model - Magnitude-Frequency Distribution

97 A problem with the simple fault model of **Figure 1** is that, observationally, larger magnitude
 98 and thus longer ruptures occur less frequently than shorter ones. One path forward for adjusting
 99 rupture length expectations is to apply a fault magnitude-frequency distribution (MFD). The
 100 exact form of the MFD appropriate to describe the recurrence of large ($>M6 - 6.5$) earthquakes
 101 on long faults remains a topic of discussion, but the power-law Gutenberg-Richter (GR) MFD
 102 provides a relevant reference. In a GR distribution, the number of earthquakes equal or
 103 exceeding some magnitude \mathbf{M} is given by $\log N(\mathbf{M}) = a - b * \mathbf{M}$. Typically, and in California, the
 104 value of b is found to be near 1. We convert model lengths to magnitudes using $\mathbf{M}-L$
 105 relationships of Anderson et al. (2017). The value of a is not required because of the condition
 106 that the event has initiated, and only the relative frequency of larger events is thus of interest.

107 The effect of assuming the power law frequency distribution is to progressively decrease
 108 probabilities with increasing rupture length (**Figure 2b**).

109 **Table 1** lists the predicted relative frequencies of events by magnitude. To tabulate length or
 110 magnitude), $N(\mathbf{M})$ includes all events of a given length. For example, three ruptures including S_0
 111 have length 21 km ($S_2-S_1-S_0$, $S_1-S_0-S_{-1}$, and $S_0-S_{-1}-S_{-2}$). The frequency of any one of the three
 112 (absent other information) is thus from **Table 1** $N(\mathbf{M})=0.110/3$. **Table 1** immediately provides a
 113 useful reference. For example, only 25% ruptures are predicted to grow to occupy a second
 114 subsection, and only 2% would go on to become an **M** 7.0 event.

115 **Table 1.** Final rupture length and frequency of length given a 7-km initial rupture.

Length (km)	7	14	21	28	35	42	49	56	63
Mw	5.33	5.94	6.29	6.54	6.73	6.89	7.02	7.14	7.24
N(M) ratio	1.000	0.246	0.110	0.062	0.040	0.028	0.020	0.016	0.012

116

117 Modifying the Discretized Model - Fault Geometry

118 *Faults and Bends*

119 In the simple fault model of **Figure 1** rupture can proceed from one panel to the next without
 120 penalty. Empirical observations and computer models of rupture processes indicate that
 121 geometrical complexities such as steps and bends affect the probability that rupture will stop
 122 (e.g., Biasi and Wesnousky, 2016; Biasi and Wesnousky, 2017; Lettis et al., 2002; Harris et al.,
 123 1991; Lozos et al., 2011; Lozos et al., 2015). To illustrate the effect, we modify the simple fault
 124 model of **Figure 1** to include bends and steps in the fault trace (**Figure 3a**). Each rupture
 125 complexity is considered to represent a “challenge” for propagation. We qualitatively illustrate
 126 the reduction in probability arising from each challenge with the dashed lines in **Figure 3b**.
 127 Probabilities on the left side are lower than on the right because three subsection connections on
 128 the right have no bend or step to reduce the probability of continuing.

129 To quantify the effects of steps and bends, we draw on the results of Biasi and Wesnousky
 130 (2016, 2017). Considering step widths first, Biasi and Wesnousky (2016) measured steps in
 131 mapped historic surface ruptures. Where faults were mapped beyond the ends of surface rupture,
 132 step widths at the ends of ruptures were also measured. For a given step width, the ratio of the

133 number of ruptures that passed to the number of that size that stopped rupture at an end is
 134 defined as the passing ratio (**Figure 4a**). An approximately linear dependence of this ratio on
 135 step width is observed for steps from 1 to 6 km. Ruptures are observed to stop or pass through
 136 steps of 3 km with approximately equal frequency. A similar passing ratio relationship was
 137 observed for bends in surface ruptures, where the size of the angle in the surface trace is
 138 observed (**Figure 4b**). For bends, observations show that bends in a fault trace $<15^\circ$ are passed
 139 over twice as often as they stop rupture while bends of 31° are twice as likely to stop rupture as
 140 to be passed.

141 Passing ratios for steps and bends in **Figures 4a and b** are converted to probabilities in
 142 **Figures 4c and d**, respectively. P_{ab} and P_{as} are the probabilities that a bend or step, respectively,
 143 will arrest rupture. The complimentary probabilities, $P_{pb}=1-P_{ab}$ and $P_{ps}=1-P_{as}$, respectively, are
 144 interpreted as the probability that a rupture will pass beyond the bend or step. For steps smaller
 145 than 1 km, a linear extrapolation is applied in **Figure 4c**. It is assumed that no probability
 146 decrease should be applied to rupture continuance when no step is present between panels. The
 147 discontinuity in slope at a width of 1 km is considered to be an artifact of insufficient data (Biasi
 148 and Wesnousky, 2016) that might be resolved with further study. For the probability of stopping
 149 at bends shown in **Figure 4d**, a smoother extrapolation has been used because the range of
 150 estimates in passing ratio for angles smaller than 10 degrees is less well defined. We consider a
 151 bend of 0 (no bend) to associate with a penalty of 0.

152 The probability curves of **Figures 4c and 4d** provide the means to quantify consequences of
 153 bends and steps of a discrete fault model such as is shown in **Figure 3**. The probability of a
 154 rupture lengthened by one subsection is smaller by the “penalty” from the step or bend, applied
 155 as a product. The cumulative effect of these penalties for bends and steps means that long,
 156 complex ruptures should be rare compared to their incidence on geometrically simpler faults.

157 *Expanding to consider UCERF3 model*

158 The model in **Figure 4** can be extended to the active fault system of California using the fault
 159 model in UCERF3 (**Figure 5**). The discrete fault elements are called “subsections”. They
 160 extend in depth to the base of the local seismogenic zone, and half that (i.e. 5-7 km) in strike
 161 length. Fault subsections in UCERF3 can have multiple sub-planes, but to be consistent in scale
 162 size with the measurements in Biasi and Wesnousky (2016, 2017), orientations are represented
 163 by an average single dip and dip direction. We estimate the dip direction using the strike defined

164 by end points of the subsection. In UCERF3, ruptures consist of a sequence of two or more
 165 subsections. Ruptures are limited to single paths with no discontinuities greater than the
 166 maximum step size, and no bifurcations (“Y”-shaped ruptures). The complete set of ruptures
 167 receiving rate estimates was defined using rules for geometric compatibility in Milner et al.
 168 (2013). The rupture rates themselves were estimated using a Monte-Carlo-based inversion (Field
 169 et al., 2014). Rupture geometric complexity was not applied as an a priori probability constraint
 170 in the UCERF3 inversion.

171 The UCERF3 fault model contains the necessary framework to estimate probabilities of
 172 eventual length for any rupture on the fault system detected earthquake early warning. If the
 173 initial alert is identified with any subsection in the UCERF3 fault model, the effects of bends and
 174 steps on rupture extension can be calculated using the probabilities in **Figures 4c and d**. Step
 175 distances between subsections are calculated from the separation of fault panels based on the
 176 latitudes and longitudes of the ends of the subsections. The angle between fault subsections is
 177 computed in 3-D using the average dip and computed dip direction parameters of the
 178 subsections. The conditional probability $P_k(L)$ of rupture length L under step and bend effects
 179 given initiation at subsection k , is

180 Eqn 1.
$$P_k(L) = \prod P_{sb_i}$$

181 where the P_{sb_i} is the step or bend probability connecting adjacent subsections in the rupture and
 182 product is over pairs of subsections that comprise length L . Equation 1 applies to unilateral
 183 rupture from the initial subsection. For any specific bi-lateral rupture, Eqn 1 is applied once in
 184 each direction to cover the full rupture extent, and the probabilities associated with the two
 185 directions are multiplied. With application of **Equation 1** to successively longer ruptures, the
 186 accumulation of step and bend penalties produces a monotonically declining probability of
 187 rupture length.

188 We illustrate the application of step and bend passing probabilities to estimate rupture length
 189 probabilities with two examples from southern California (**Figures 6 and 7**). The first example
 190 assumes the earthquake starts at the southeastern end of the San Andreas fault at Bombay Beach
 191 (star), and rupture extends unilaterally northwest (**Figure 6**). In **Figure 6**, subsection
 192 intersections for the SAF and SJF are shown as dots. From the alert location, the individual bend

193 and step penalties for rupture are computed separately using the geometries of each subsection
 194 intersection. The individual bend and step passing probabilities are shown in **Figure 7a** (circles
 195 and + symbols, respectively), and the solid line shows their joint application. Cumulative
 196 applications of each using **Eqn 1** are shown in **Figure 7b**. We take probabilities of length in our
 197 interpretations from cumulative joint probability curve. The SAF northwest from Bombay
 198 Beach is relatively straight and smooth. The first significant bend and step complexities are
 199 encountered 13 subsections NW at the intersection with the Mill Creek SAF fault section. Other
 200 SAF section transitions are indicated in Figure 6. The decline in propagation probabilities north
 201 of the Coachella section is consistent with the progressive CCW rotation of fault strike on the
 202 Mill Creek to a less favorable orientation for through rupture. Only 5% of ruptures starting on
 203 the Coachella section are predicted to get past the Mill Creek section to reach eastern San
 204 Bernardino, only 2.5% continue to the near SE end of the Mojave South section (**Figure 7b**), and
 205 only 0.2% would rupture “wall-to-wall” from Bombay Beach to Parkfield. Based on fault
 206 geometry, ruptures that start in the southeast end of the San Andreas fault should rarely reach to
 207 the eastern edge of metropolitan Los Angeles at San Bernardino.

208 In the second example, the rupture starts on the San Jacinto fault at the Casa Loma step over
 209 (**Figure 6; Figure 8**). In this case, rupture might extend northwest or southeast. Because
 210 probabilities in Equation 1 are conditioned on the alert location, probabilities of the NW and SE
 211 extents are independent, and thus can be considered separately. In the UCERF3 fault model, the
 212 SJF can connect NW to the San Bernardino North SAF two ways, over 3 subsections of the Lytle
 213 Creek fault (**Figure 8a, b**) or continue 3 subsections further on the SJF (**Figure 8c**). Based on
 214 fault geometry, the direct connection is a more likely path for through ruptures, though neither is
 215 very likely to actually continue on the Mojave South section (5.8% vs. 2.7%). Lozos et al.
 216 (2015) and Lozos (2016) have studied rupture propagation through this intersection and found
 217 that it is sensitive to poorly resolved details of the fault system geometry. For rupture extending
 218 to the SE on the SJF, decrements in probability correspond to recognized section boundaries
 219 (**Figure 8d**). Anza and Coyote Creek sections are relatively straight, with little geometric basis
 220 for rupture arrest, while curvature of the Borrego fault (**Figure 6**) causes a progressive decrease
 221 in probability of through rupture. The probability of any given bilateral rupture extent given a
 222 starting alert near the Casa Loma stepover would be the product of probability of the
 223 corresponding NW and SE extents.

224 **In Figures 7 and 8** we so far have discussed conditional probabilities of length on a single
 225 rupture path. This may be sufficient for some purposes. However, if conditional probability of
 226 length or magnitude is required regardless of path, an accounting must be made of probabilities
 227 at branch points. As long as the paths are independent alternatives, probabilities of a given
 228 rupture length or magnitude can be combined by weighting by their relative geometric
 229 probabilities at the branch point. Using the example in **Figure 8** of connection from the SJF to
 230 the SAF directly versus by Lytle Creek, the last common point is on the San Jacinto San
 231 Bernardino strand (SJSB, **Figures 8b and c**). Staying on the SJF involves a bend probability of
 232 0.76, and no step penalty. Jumping to the Lytle Creek fault involves a slightly larger bend
 233 penalty of 0.64 and a small step with penalty, 0.91. Combining, gives probabilities of 0.76 vs.
 234 0.58, respectively. Thus, based on fault geometric parameters, the direct connection is preferred.
 235 Probabilities of length on the direct connection path would be weighted by $0.76/(0.76+0.58) =$
 236 57% vs. 43% for connection by Lytle Creek. Weighting of this sort applies to length or
 237 magnitude accumulated on distinct branches. In this case, the alternate paths meet on the Mojave
 238 South section. NW of that intersection, the probabilities of length in **Figures 8b and 8c** can be
 239 summed. Alternative weighting approaches are discussed in a later section.

240 UCERF3 Rupture Length Predictions

241 If rupture probabilities are available for all possible ruptures and paths, these probabilities
 242 can provide a third basis for the conditional probability of rupture length given EEW initiation.
 243 Such probabilities are available for California from UCERF3 (Field et al., 2014). From the
 244 complete set of ruptures and probabilities, it is possible to extract subsets for a desired path and
 245 starting subsection. We illustrate this process for the San Jacinto fault starting point considered
 246 previously. We extract all ruptures in the UCERF3 Fault Model 3.1 NW and having one end at
 247 the Casa Loma step, and plot their annual rates of occurrence (star symbols, **Figure 9a**). There
 248 are 769 ruptures with this geometry. The solid line above these points summarizes rupture rates
 249 in bins of 0.1 **M** units. This line represents the incremental magnitude-frequency curve of all
 250 ruptures with one end at the Casa Loma step over. When the logarithmic rate axis is considered,
 251 it is seen that the greatest weight (probability of occurrence) is on ruptures of **M** 7.5 or greater.

252 The assumption that the earthquake has started provides a basis to project UCERF3 annual
 253 probabilities into a conditional probability of length function. The UCERF3 rupture set was

254 constructed to give rates for all possible ruptures in the discretized fault model, so the subset
255 with an end at the Casa Loma step over defines a total probability for ruptures with that
256 geometry. Before rupture starts, the probability of any rupture in the set is small, but once we
257 say the Casa Loma step subsection is at one end, with probability 1, the final rupture will be one
258 from the set.

259 The annual rates of occurrence shown for ruptures shown in **Figure 9a** assume that rupture
260 could nucleate anywhere on their length. For the EEW case, the nucleation point is a specific
261 case. To adjust rates for our constrained nucleation point, we assume the earthquake might
262 nucleate with equal likelihood in any given subsection of a rupture. We thus reduce the annual
263 probability of occurrence for each rupture in **Figure 9a** by $1/n$ where n is the number of
264 subsections in the rupture. The dashed line of **Figure 9b** incorporates this reduction and so
265 represents the UCERF3-based probability of rupture length for unilateral rupture northwest from
266 the Casa Loma step over. The result is shown in terms of probability of earthquake magnitude in
267 **Figure 9c**. In terms of expectations for length, 18% that start at the Casa Loma step over are
268 expected to reach 70 km in length and **M** 7.1. About 16% will continue over 200 km, as **M** 7.6
269 or larger events. This compares with a probability of 5.4% (summing **Figures 8b** and **8c** at 30
270 subsections) based on geometry alone.

271 The UCERF3 rupture model also supports tracking of probability of length or magnitude
272 through bifurcations in the fault. In **Figure 9**, we considered probability of length without
273 specifying exactly which fault(s) the rupture might occupy. Thus, in the set shown, some
274 ruptures join the SAF from the SJF both directly to the SAF north San Bernardino section, and
275 alternately on the Lytle Creek section. Where it is desirable to track such distinctions, the
276 process with **Figure 9** is repeated, but with the rupture set separated by fault branch.
277 Probabilities for each branch at the “Y” are estimated according to the total UCERF3 probability
278 of ruptures that continue. Similarly, bilateral length probabilities conditioned on the initiation
279 point are formed by gathering the SE and NW sets separately in the example of **Figure 8**, then
280 multiplying the probabilities of length on either side. The eventual magnitude probabilities,
281 however, must be scaled from the combined lengths using a relationship such as in Anderson et
282 al. (2017).

283 Discussion

284 Fault-geometric passing probabilities provide an empirical basis for estimating potential
285 rupture lengths given an initiation point on the fault system. Probabilities reflect a “time-
286 independent” estimate, using averages over many historical ruptures, in the same sense as the
287 passing probabilities used to create them. And although we have motivated the research by its
288 application to EEW, conditional length estimates are equally applicable in other contexts where
289 probabilities of rupture extent are needed for hazard scenarios and response planning.

290 We find for representative nucleation points on southern California’s most active faults that
291 realistic probabilities of rupture length can be formed directly from probabilities at geometric
292 complexities. The relatively low probabilities that we find for a rupture extending from the
293 southernmost San Andreas fault into San Bernardino or beyond (Figure 7) are consistent with
294 geologic and dynamic modeling assessments that such a rupture should be rare. For rupture NW
295 from the northern San Jacinto fault (**Figure 8**) we find lower probabilities than from UCERF3 by
296 about a factor of 2 that rupture should extend onto the San Andreas fault. For long, straight
297 faults, some adjustment of rupture probabilities beyond fault-geometric passing probabilities
298 might be considered if shorter ruptures are known to be more likely than long ones. Reasonable
299 adjustments can be achieved with a Gutenberg-Richter or similar fault system magnitude-
300 frequency distribution. Alternatively, the straight portions of faults with no notable geometric
301 complexity may give a physical basis for some measure of characteristic earthquake behavior.

302 For long ruptures, probability estimates of rupture length or eventual rupture magnitude will
303 require either picking a single fault rupture path, or a means to include probabilities across fault
304 branching. We illustrated an approach using relative weights based on geometric favorability at
305 the intersection providing alternate paths NW from the San Jacinto fault (**Figure 8**). If there
306 were further branches, this procedure could be applied recursively. One might alternatively
307 weight branch probabilities on the basis of relative slip rates of the branches. Using the
308 UCERF3 fault model, slip rates on the SJF and Lytle Creek where they split are 9.0 mm/yr and
309 1.8 mm/yr, respectively. On this basis, a weighting is found of 83% vs. 17%, respectively,
310 compared to 57% vs. 43% found from geometry alone. A related division might be calculated by
311 summing rupture rates on each branch from the UCERF3 time-independent model.

312 For specific branch points, paleoseismic data might also provide a basis to adjust respective
313 weightings of branches. Schwartz et al. (2012) show that the eastern extent of the Denali fault
314 had a more recent large surface rupture earthquake on it than the Totchunda fault near their
315 intersection. When the Denali earthquake rupture propagated east, it took the less geometrically
316 favored branch, they infer, because of the more recent previous Denali event. While potentially
317 useful at individual branches, the application of paleoseismic data in this way would be situation-
318 specific. For California, a generalization of this type of data is available through the time-
319 dependent version of UCERF3 (Field et al., 2015). Its use in estimating conditional probabilities
320 of rupture length reserved for future research.

321 Beside probability of length or magnitude, other questions might be asked, such as the
322 probabilities of magnitude for ruptures that could reach a certain point, such as an urban area.
323 For a conditional probability question such as this, one must consider all combinations of SE and
324 NW extent affecting the city. This would require a certain level of bookkeeping, as illustrated
325 with **Figure 1**, but not comprise an entirely new approach.

326 For EEW applications, probabilities of length and/or magnitude from any initiation point in
327 the fault model could readily be precompiled. If precompiled, then during an EEW alert, length
328 probabilities can be accessed very quickly by means of look-up table. Such a lookup will not
329 take the place of dynamic estimates of magnitude such as are provided by the FinDer algorithm
330 (Bose et al., 2012, 2015), but length probabilities may be useful for alert area updates.

331 We motivated this research by considering probabilities of rupture length from an EEW
332 initial alert. During an EEW rupture, precision in the estimate will be secondary to the need to
333 quickly extend the alert area for a growing rupture. If the question is instead, how do we set
334 policy for an alert area given a growing rupture, the methods developed here could inform the
335 discussion. For example, if an alert earthquake reaches M6, say, on the SE San Andreas fault,
336 are the growth probabilities high enough that all of Los Angeles should be alerted? What about
337 an alert on the southern San Jacinto fault? Are the differences in probability large enough to
338 have fault-specific policies? The methods outlined here can provide input to those decisions.

339 Beyond application to rupture length estimates, fault-geometric passing probabilities provide
340 complimentary model evaluation metrics for a future UCERF model. UCERF3 ruptures start
341 with no a priori probability per se. If a rupture passes basic geometric compatibility tests (Milner
342 et al., 2013), nothing downstream in the rupture rate inversion distinguishes simple vs.

343 geometrically complex ruptures. Mathematical relationships implementing fault geometric
344 passing probabilities might be formulated, for example, to constrain the ratio of through ruptures
345 to ruptures that stop at a geometric feature. Alternatively, fault-geometric probabilities could be
346 used as a complimentary tool to identify ruptures that pass the Milner et al. (2013) screening, but
347 include multiple, unfavorable geometric intersections and thus could be culled from the rupture
348 set. Shaw et al. (2018) show as long as fault slip rates are matched in the rupture set, hazards
349 and ground motion estimates will match the full rupture set. A smaller input rupture set would
350 improve computational performance of the rate inversion. Finally, instead of using fault
351 geometric probabilities as inputs to the inversion, they could be used to compare with inversion
352 results. The UCERF3 model has been difficult for geologists to evaluate (e.g., Schwartz, 2018)
353 because virtually all available geologic data are used as inputs to the inversion. Once the data
354 are fit by the inversion, little independent data remain to evaluate the resulting model.
355 Geometrically based passing probabilities cannot directly replace a rupture rate inversion, but
356 they do make specific, physically grounded predictions of the relative rates of long and short
357 ruptures and these data are not inputs to the UCERF3 inversion. Summarizing, step and bend
358 complexities model geometry well, without reference to slip rate, and UCERF3 fits slip rate
359 without reference to geometric complexity.

360 Conclusion

361 A fault-geometric approach is presented to estimate the conditional probabilities of rupture
362 length and/or magnitude, based on probabilities of passing bend and step structures. Fault
363 geometric complexities, when translated to probabilities of rupture arrest, comprise challenges a
364 rupture encounters serially in order to increase in length. The probability of length is thus the
365 product of the complimentary probabilities of continuing. Long and complex ruptures are, as a
366 consequence, less frequent, conforming to empirical observation. For example nucleation points
367 on the San Andreas and San Jacinto faults in southern California, the derived probability of
368 length estimates conform to expectations that ruptures are likely to be arrested **in by** the
369 significant change in fault strike of the Mill Creek and eastern north San Bernardino sections.
370 Only 2% of ruptures starting at Bombay Beach are predicted to extend onto the southern Mojave
371 section of the fault. Based on fault geometric complexity, fewer than 10% that initiate on the
372 NW San Jacinto fault would proceed onto the southern San Andreas fault.

373

374 One may also extract conditional length probabilities directly from the UCERF3 rupture
375 rates. This use of UCERF3 assumes that the conditional probability of rupture length given a
376 nucleation point can be interpreted from the time-independent rupture rate forecast. In a point
377 comparison for the northern San Jacinto fault, conditional probabilities of length systematically
378 favor longer ruptures than from geometric complexity. Fault-geometric probabilities could also
379 play a role in future UCERF models, either as a data constraint, a compliment to model
380 construction, or as a tool to evaluate inversion results. Fault-geometric features exert physically
381 significant effects on ruptures, so their inclusion in future UCERF models would be a step
382 toward a more physically based rupture rate model.

383 In an earthquake early warning context, the methods developed here provide a basis to
384 estimate where a rupture may go, and with what probabilities. These probabilities are readily
385 compiled in advance for any given starting subsection in the fault model, in effect covering likely
386 nucleation locations for large earthquakes anywhere in the California fault network. These
387 probabilities could be used before the event to advise policy about alerting extent for different
388 faults. Operationally, pre-compiled probabilities could quickly be accessed by the EEW system
389 when an earthquake has initiated. As an immediately useful result, we find that an earthquake
390 that initiates at Bombay Beach on the SE end of the San Andreas fault only reaches San
391 Bernardino about 5% of the time, the point at which modeling suggests a major risk to Los
392 Angeles.

393 Data Sources

394 All data used in this paper are from published sources in cited references.
395

396 Acknowledgements

397 This research was supported by the Southern California Earthquake Center Awards 17064
398 and 12012 (Contribution No. XXXX). SCEC is funded by NSF Cooperative Agreement EAR-
399 1600087 & USGS Cooperative Agreement G17AC00047. Center for Neotectonics Studies
400 Contribution #XX.

401

402 **References**

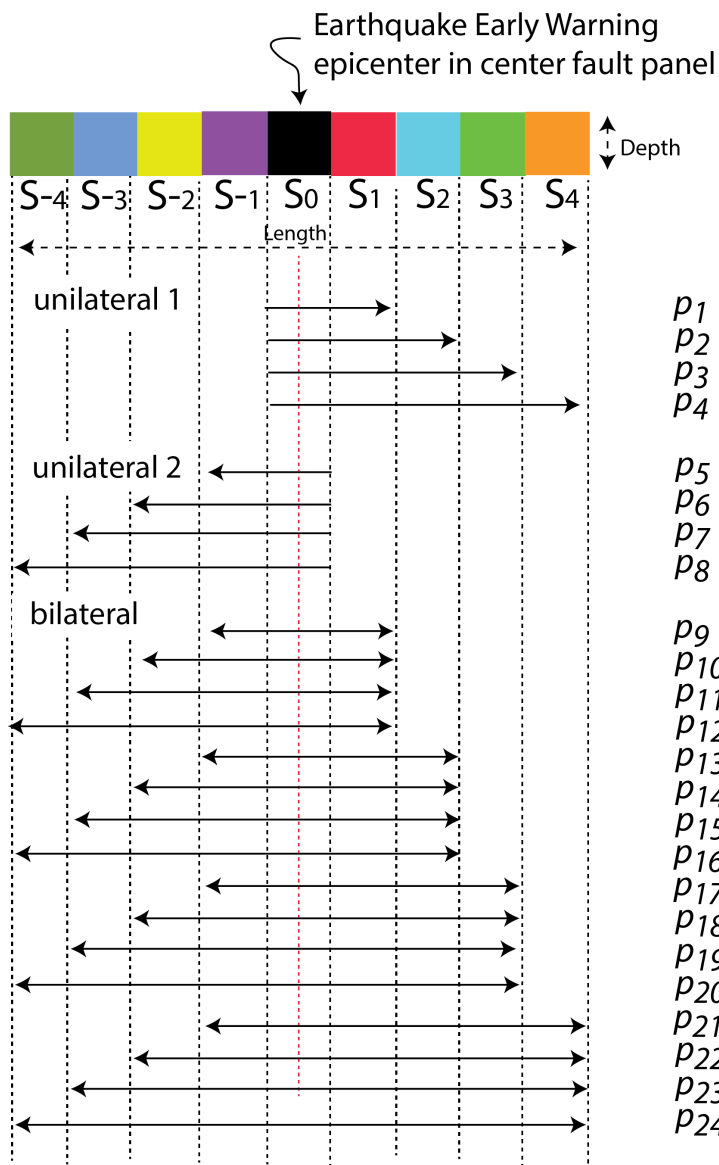
- 403 Allen, R. M. and H. Kanamori, 2003. The potential for earthquake early warning in Southern
 404 California, *Science* 300, 786-789.
- 405 Allen, R. M., P. Gasparini, O. Kamigaichi and M. Böse, 2009. The status of earthquake early
 406 warning around the world: An introductory overview, *Seismol. Res. Lett.*, 80, 682-693.
- 407 Anderson, J. G., G. P. Biasi and S. G. Wesnousky, 2017. Fault-scaling relationships depend on
 408 the average fault-slip rate. *Bull. Seismol. Soc. Am.*, 107, 2561-2577.
- 409 Biasi, G. P. and S. G. Wesnousky, 2016. Steps and gaps in ground ruptures: empirical bounds on
 410 rupture propagation, *Bull. Seismol. Soc. Am.*, 106, 1110-1124.
- 411 Biasi, G. P. and S. G. Wesnousky, 2017. Bends and ends of surface ruptures, *Bull. Seismol. Soc.*
 412 *Am.*, 107, 2543-2560.
- 413 Böse, M., C. Felizardo, and T. H. Heaton (2015). Finite-fault rupture detector (FinDer): Going
 414 real-time in Californian ShakeAlert system, *Seismol. Res. Lett.* 86, 1692-1704.
- 415 Böse, M., T. H. Heaton, and E. Hauksson (2012). Real-time finite fault rupture detector (FinDer)
 416 for large earthquakes, *Geophys. J. Int.*, 191, 803–812.
- 417 Chung, A. I., I. Henson, and R. M. Allen (2019). Optimizing earthquake early warning
 418 performance: ElarmS-3, *Seismol. Res. Lett.*, 90, 727-743.
- 419 Cochran, E. S., J. Bunn, S. E. Minson, A. S. Baltay, D. L. Kilb, Y. Kodera, and M. Hoshihara
 420 (2019). Event detection performance of the PLUM earthquake early warning algorithm in
 421 southern California, *Bull. Seismol. Soc. Am.*, 109, 1524-1541.
- 422 Cooper, J.D., 1868. Cooper J. D. San Francisco Daily Evening Bulletin November 3.
- 423 Field, E. H., T. H. Jordan, M. T. Page, K. R. Milner, B. E. Shaw, T. E. Dawson, G. P. Biasi, T.
 424 Parsons, J. L. Hardebeck, A. J. Michael, R. J. Weldon, P. M. Powers, K. M. Johnson, Y. H.
 425 Zeng, K. R. Felzer, N. van der Elst, C. Madden, R. Arrowsmith, M. J. Werner, and W. R.
 426 Thatcher, 2017. A synoptic view of the Third Uniform California Earthquake Rupture
 427 Forecast (UCERF3). *Seismol. Res. Lett.*, 88, 1259-1267.
- 428 Field, E. H., G. P. Biasi, P. Bird, T. E. Dawson, K. R. Felzer, D. D. Jackson, K. M. Johnson, T.
 429 H. Jordan, C. Madden, A. J. Michael, K. R. Milner, M. T. Page, T. Parsons, P. M. Powers, B.
 430 E. Shaw, W. R. Thatcher, R. J. Weldon, and Y. Zeng (2015). Long-term, time-dependent

- 431 probabilities for the Third Uniform California Earthquake Rupture Forecast (UCERF3), *Bull.*
 432 *Seism. Soc. Am.* 105, 511–543.
- 433 Field, E. H., R. J. Arrowsmith, G. P. Biasi, P. Bird, T. E. Dawson, K. R. Felzer, D. D. Jackson,
 434 K. M. Johnson, T. H. Jordan, C. Madden, A. J. Michael, K. R. Milner, M. T. Page, T.
 435 Parsons, P. M. Powers, B. E. Shaw, W. R. Thatcher, R. J. Weldon, R.J., and Y. H. Zeng,
 436 2014. Uniform California Earthquake Rupture Forecast, Version 3 (UCERF3) -The time-
 437 independent model. *Bull. Seismol. Soc. Am.*, 104, 1122-1180.
- 438 Harris, R. A., R. J. Archuleta and S. M. Day, S.M., 1991. Fault steps and the dynamic rupture
 439 process - 2-D numerical simulations of a spontaneously propagating shear fracture. *Geophys.*
 440 *Res. Lett.* 18, 893-896.
- 441 Heaton, T. H., 1985. A model for a seismic computerized alert network. *Science* 228, 987-990.
- 442 Kanamori, H., E. Hauksson, and T. Heaton, 1997. Real-time seismology and earthquake hazard
 443 mitigation, *Nature* 390, 461-464.
- 444 Kanamori, H., P. Maechling, and E. Hauksson, 1999. Continuous monitoring of ground-motion
 445 parameters. *Bull. Seismol. Soc. Am.*, 89, 311-316.
- 446 Kanamori, H., 2005. Real-time seismology and earthquake damage mitigation, *Ann. Rev. Earth*
 447 *and Planet. Sci. Lett.*, 33, 195-214.
- 448 Kodera, Y. (2018). Real-time detection of rupture development: Earthquake early warning using
 449 P waves from growing ruptures, *Geophys. Res. Lett.* 45, 156–165.
- 450 Kohler, M. D., E. S. Cochran, D. Given, S. Guiwits, D. Neuhauser, I. Henson, R. Hartog, P.
 451 Bodin, V. Kress, S. Thompson, C. Felizardo, J. Brody, R. Bhadha, and S. Schwarz (2018).
 452 Earthquake early warning ShakeAlert system: West Coast wide production prototype,
 453 *Seismol. Res. Lett.*, 89, 99-107.
- 454 Lettis, W., J. Bachhuber, R. Witter, C. Brankman, C. E. Randolph, A. Barka, W. D. Page, and A.
 455 Kaya (2002). Influence of releasing step-overs on surface fault rupture and fault
 456 segmentation: Examples from the 17 August 1999 Izmit earthquake on the North Anatolian
 457 fault, Turkey, *Bull. Seismol. Soc. Am.*, 92, 19-42.
- 458 Lozos, J. C. (2016). A case for historic joint rupture of the San Andreas and San Jacinto faults,
 459 *Science Advances*, 2:e1500621, 7 p.

- 460 Lozos, J.C., D. D. Oglesby, B. Duan, and S. G. Wesnousky (2011). The effects of double fault
 461 bends on rupture propagation: A geometrical parameter study, *Bull. Seismol. Soc. Am.*, *101*,
 462 385-398.
- 463 Lozos, J. C., D. D. Oglesby, J. N., Brune, and K. B. Olsen (2015). Rupture propagation and
 464 ground motion of strike-slip stepovers with intermediate fault segments, *Bull. Seism. Soc.*
 465 *Am.*, *105*, 387-399.
- 466 Meier, M.-A., T. Heaton, and J. Clinton (2016). Evidence for universal earthquake rupture
 467 initiation behavior, *Geophys. Res. Lett.*, *43*, 7991-7996.
- 468 Milner, K., M. T. Page, E. H. Field, T. Parsons, G. Biasi, and B. E. Shaw (2013). Defining the
 469 inversion rupture set via plausibility filters, U.S.G.S Open-File Report 2013-1165, Uniform
 470 California Earthquake Rupture Forecast Version 3 (UCERF3) – The Time-Independent
 471 Model, Appendix T, 14 pp.
- 472 Nakamura, Y., 1988. On the urgent earthquake detection and alarm system (UrEDAS).
 473 *Proceedings of the Japanese National Committee of the International Association for*
 474 *Earthquake Engineering VII*, 224-238.
- 475 Noda, S. and W. L. Ellsworth (2016). Scaling relation between earthquake magnitude and the
 476 departure time from P wave similar growth, *Geophys. Res. Lett.*, *43*, 9053-9060.
- 477 Olson, E. L. and R. M. Allen (2005). The deterministic nature of earthquake rupture, *Nature*,
 478 *438*, 212-215.
- 479 Schwartz, D. P. (2018). Past and future fault rupture lengths in seismic source characterization –
 480 The long and short of it, *Bull. Seismol. Soc. Am.*, *108*, 2493-2520.
- 481 Schwartz, D. P., P. J. Haeussler, G. G. Seitz, and T. E. Dawson (2012). Why the 2002 Denali
 482 fault rupture propagated onto the Totschunda fault: Implications for fault branching and
 483 seismic hazards, *J. Geophys. Res.*, *117*, B11304.
- 484 Shaw, B. E., K. R. Milner, E. H. Field, K. Richards-Dinger, J. J. Gilchrist, J. H. Dieterich, and T.
 485 H. Jordan (2018). A physics-based earthquake simulator replicates seismic hazard statistics
 486 across California, *Science Advances*, *4*, eaau0688, 9 pp.
- 487 Trugman, D. T., M. T. Page, S. E. Minson, and E. S. Cochran (2019), Peak ground displacement
 488 saturates exactly when expected: Implications for earthquake early warning, *J. Geophys. Res.*
 489 *Solid Earth*, *124*, 4642-4653.

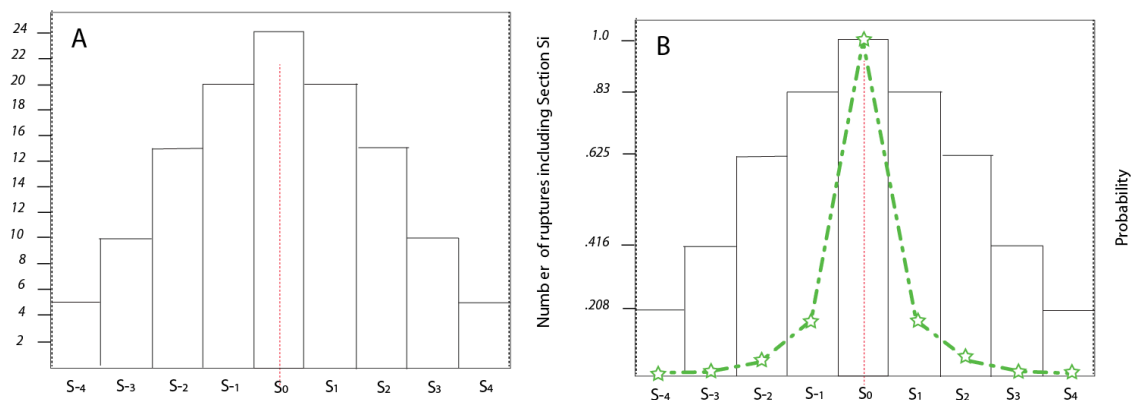
- 490 Wu, Y.M. and T. L. Teng, 2002. A virtual subnetwork approach to earthquake early warning.
491 *Bull. Seismol. Soc. Am.*, 92, 2008-2018.
- 492 Wu, Y. M. and H. Kanamori, 2005. Rapid assessment of damage potential of earthquakes in
493 Taiwan from the beginning of P waves. *Bull. Seismol. Soc. Am.*, 95, 1181-1185.
- 494 Wu, Y. M., H. Kanamori, R. M. Allen and E. Hauksson, 2007. Determination of earthquake
495 early warning parameters, tau(c) and P-d, for southern California. *Geophys. J. Int.*, 170, 711-
496 717.
- 497 Wu, Y. M. and H. Kanamori, 2008. Development of an earthquake early warning system using
498 real-time strong motion signals. *Sensors*, 8, 1-9.
- 499 Yamada, T. and S. Ide (2008). Limitation of the predominant-period estimator for earthquake early
500 warning and the initial rupture of earthquakes, *Bull. Seismol. Soc. Am.*, 98, 2739-2745.
501
502

503
504
505



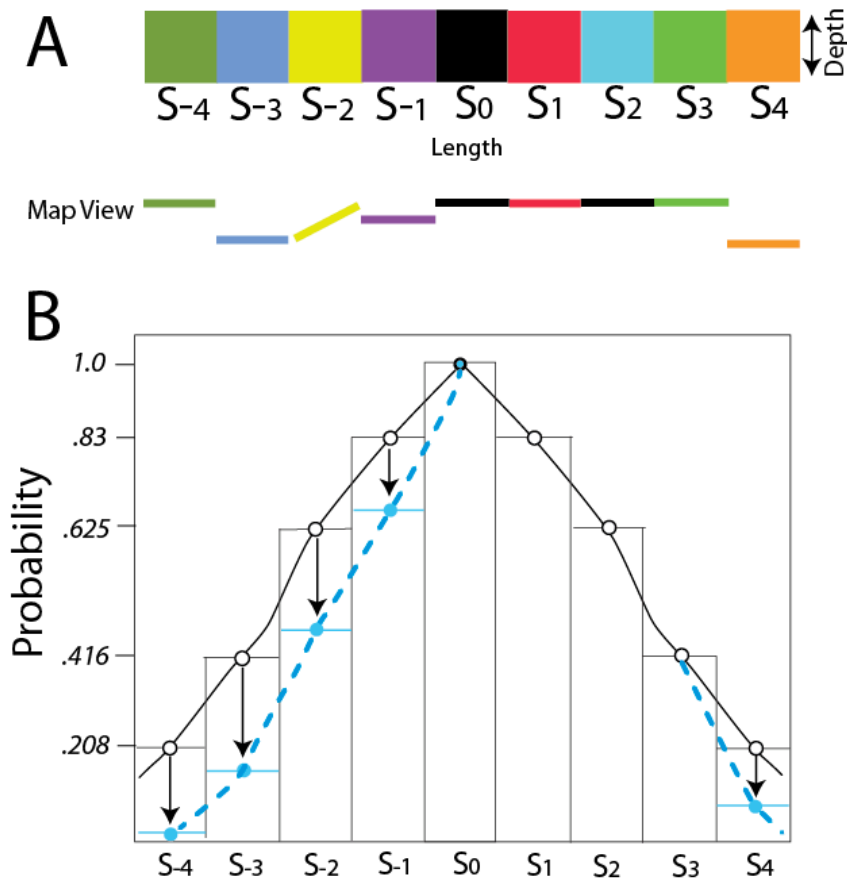
506
507
508
509
510
511
512
513

Figure 1. Illustration of single fault composed of 9 panels (subsections) illustrating possible rupture extents for an earthquake initiating in central panel S₀. The probability of any given rupture is p_i.



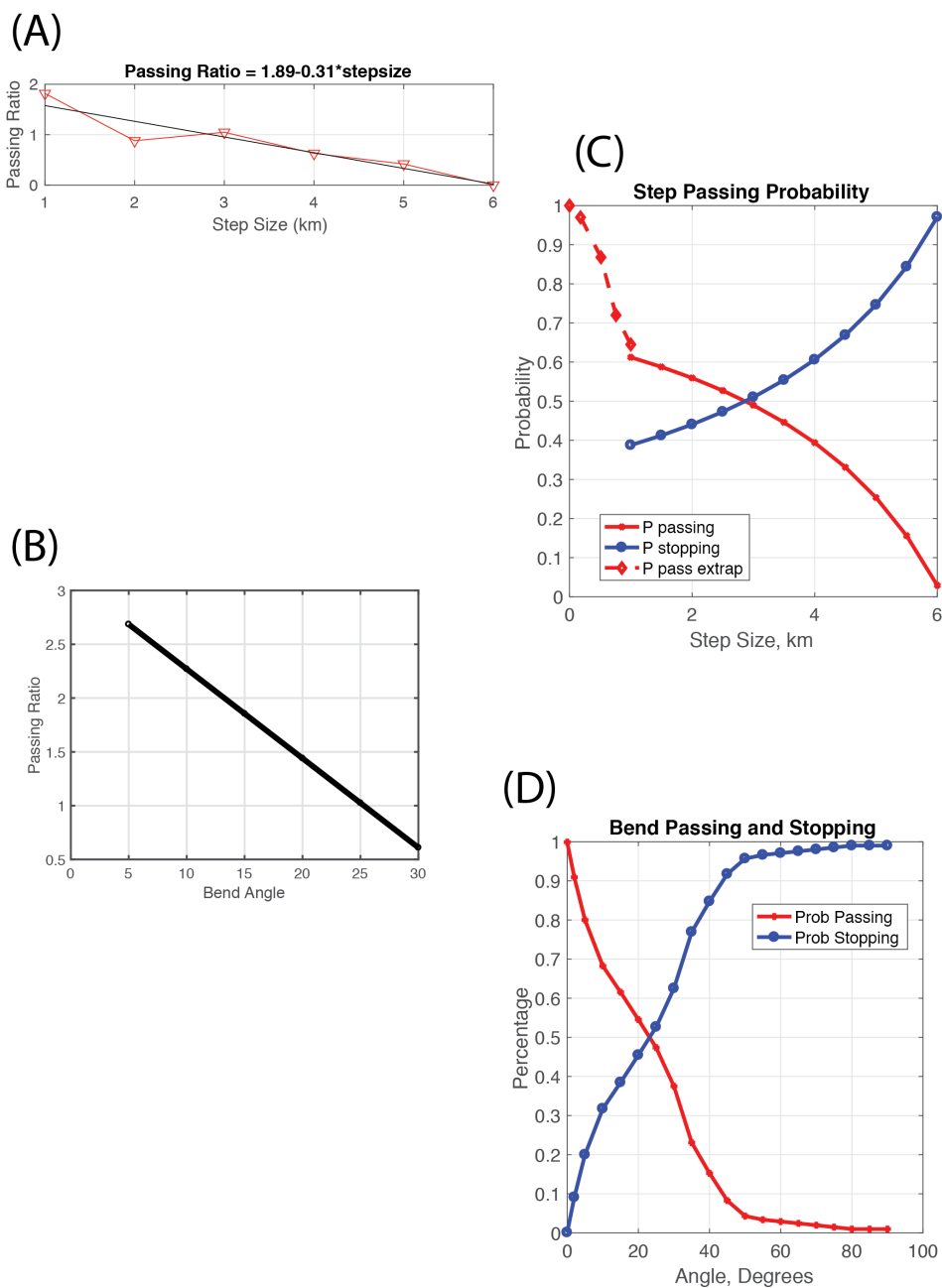
514
 515
 516
 517
 518
 519
 520
 521
 522
 523
 524
 525
 526

Figure 2. (A) Histogram showing the number of ruptures each subsection could participate in. (B) Probability of a subsection being involved in rupture given rupture initiates in S_0 and each possible rupture is considered equally likely. Dashed line and stars illustrate reduction in probabilities if a power-law distribution exists among likely rupture lengths on the model fault. See text for further discussion.



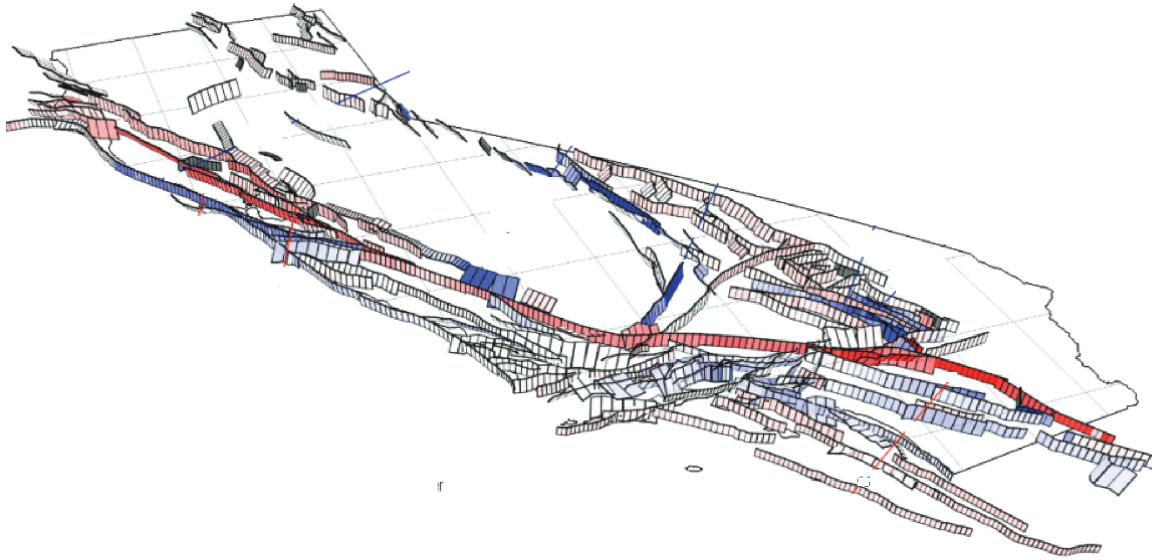
527
 528
 529
 530
 531
 532
 533
 534

Figure 3. (A) Fault model with panel boundaries containing steps and bends in fault trace. (B) The probabilities of a rupture extending from panel S₀ to others in the fault model. Open circles and solid line result if all ruptures are considered equally likely; the dashed line with filled circles reflect qualitatively the reduction in probability of length when penalties for passing are applied at panel boundary steps or bends.



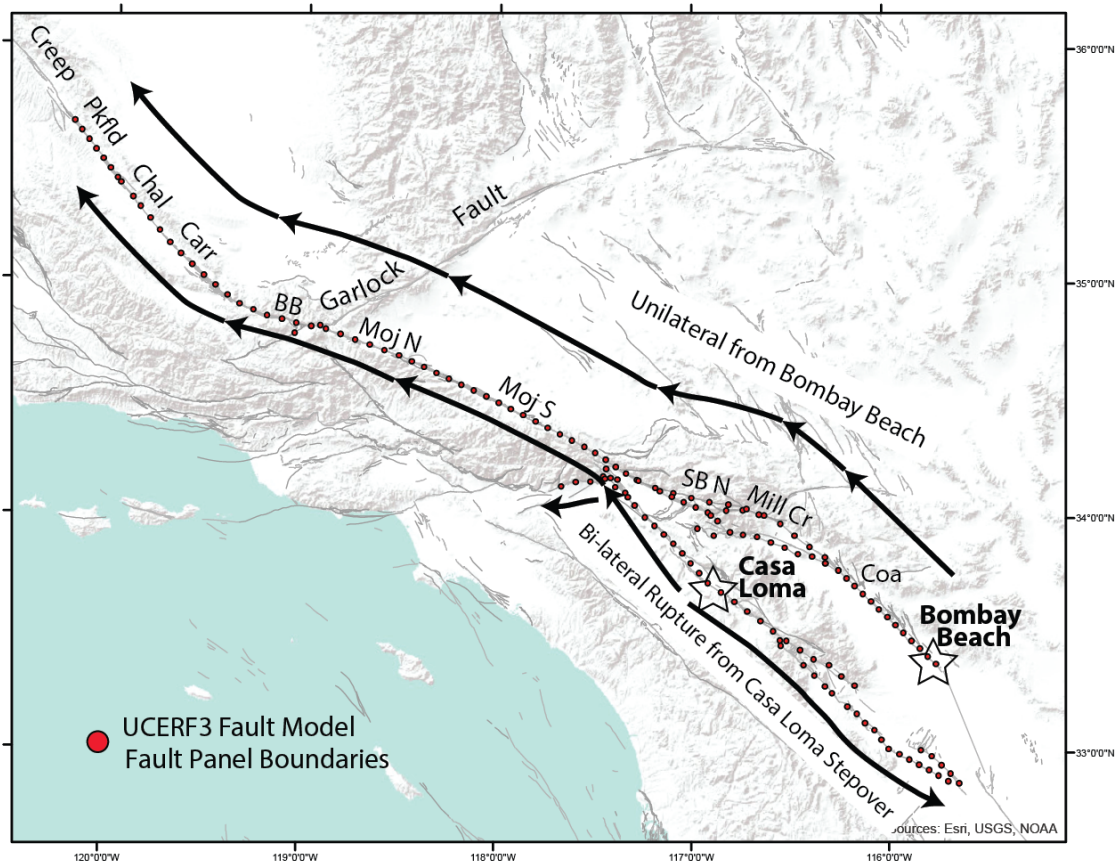
535
 536
 537 Figure 4. Passing ratios versus (A) step width and (B) bend angle, adapted from Biasi and
 538 Wesnousky 2016 and 2017, respectively. Bend and step complexities are measured between
 539 fault sections of at least 5-7 km in length. (C) Probability of passing or stopping at a step vs. step
 540 width (P_{ps} and P_{as} , respectively in the text). (D) Probability of passing or stopping at a bend of
 541 given angle in fault trace (P_{pb} and P_{ab} , respectively).
 542
 543
 544

545
546
547
548
549
550
551
552
553



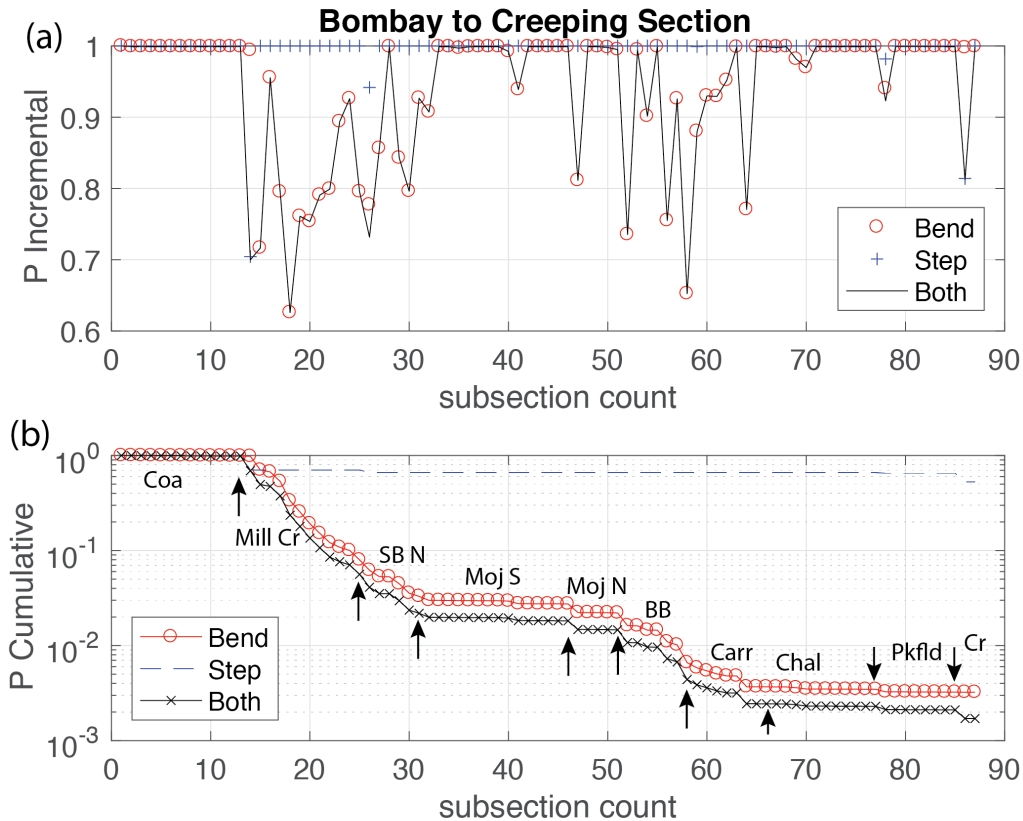
554
555
556
557

Figure 5. Discrete fault model FM3.1 from UCERF3. Faults are shaded by slip rate. Figure from Field et al. (2014).



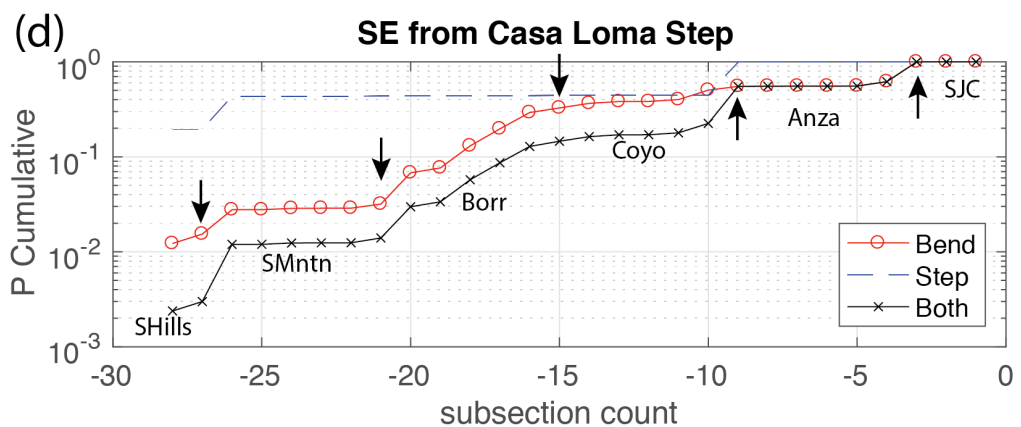
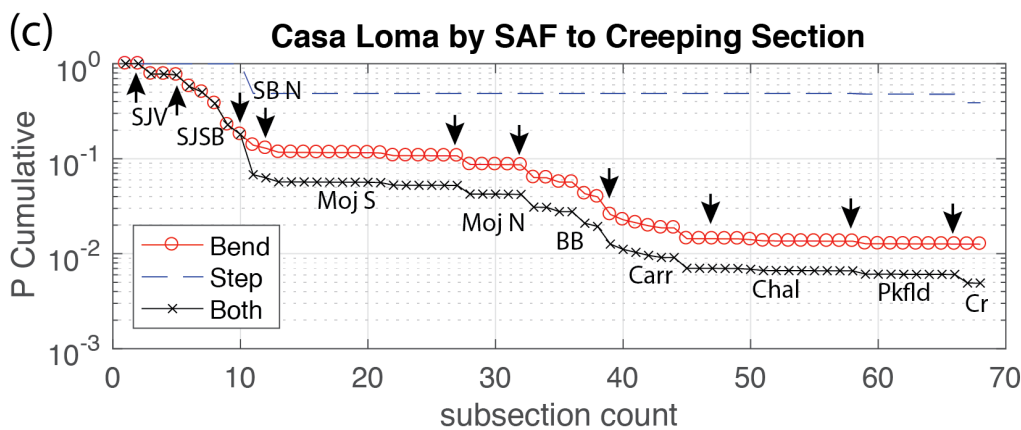
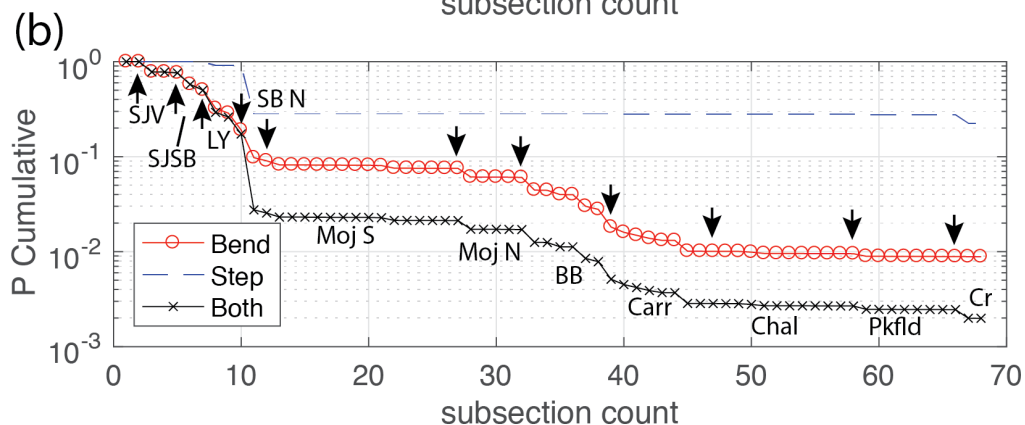
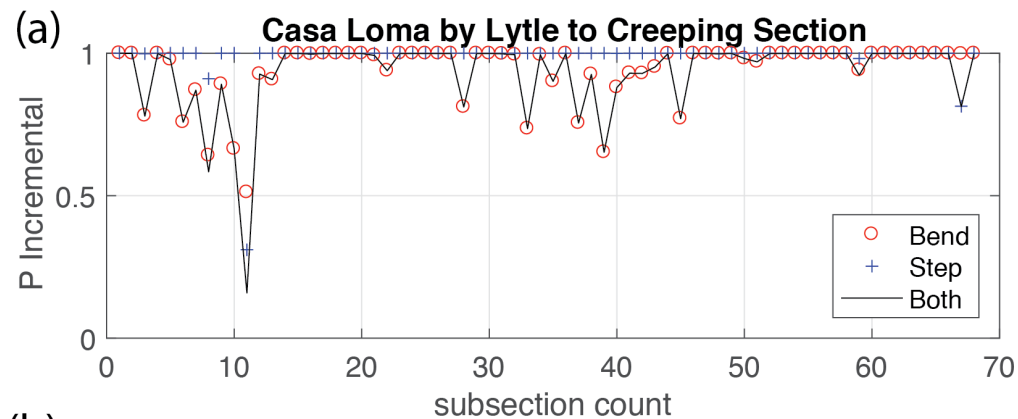
558
 559
 560
 561
 562
 563
 564
 565
 566
 567
 568

Figure 6. Example paths of rupture propagation given earthquake initiation points (stars) on two major southern California faults. Rupture starting at Bombay Beach (eastern star) is modeled on the San Andreas fault for its full length. Rupture northward on the San Jacinto fault (western star) begins at the Casa Loma stepover then transitions to the San Andreas fault either directly, or by a short section of the Lytle Creek fault. Rupture may also extend south from the Casa Loma starting point.



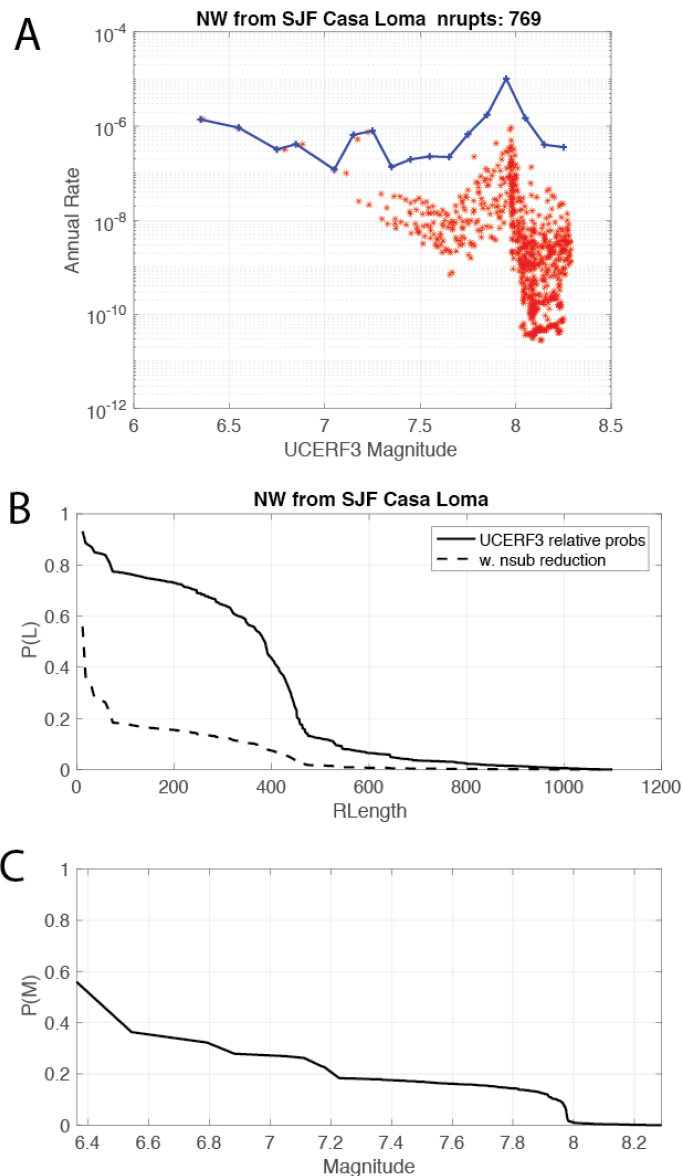
569
 570
 571
 572
 573
 574
 575
 576
 577
 578
 579
 580
 581
 582
 583
 584

Figure 7. Geometric and cumulative passing probabilities at subsection boundaries for a unilateral rupture NW from Bombay Beach. (A) Individual probabilities of continuing through subsection bend (“o”) and step (“+”) intersections. Solid line shows their joint application. Subsections are ~7 km in length. Fault portions that are straight with no steps have no geometric basis for arresting rupture. (B) Cumulative application of bend (circles) and step (dashed) penalties given initiation at Bombay Beach. “x” symbols show their joint application. Text labels indicate UCERF3 fault sections. Coa: Coachella; Mill Cr.: Mill Creek; SB N: San Bernardino North; Moj S: Mojave South; Moj N: Mojave North; BB: Big Bend; Carr: Carrizo; Chal: Cholame; Pkfld: Parkfield; Cr: SE end of creeping section. Arrows mark section intersections.



586
587
588
589
590
591
592
593
594
595
596
597
598
599
600

Figure 8. Geometric and cumulative penalties at subsection boundaries for rupture NW and SE from the San Jacinto Claremont-Casa Loma step over. (a) Individual step (“+” and dashed) and bend passing probabilities (“o”) on the paths of rupture extending (a) unilaterally NW onto the San Andreas fault by Lytle Creek to the SAF. (b) Cumulative probability of length for (a). Arrows mark section intersections. (c) Cumulative probability for an alternate path where the San Jacinto fault connects directly to the SAF directly from the San Bernardino strand of the SJF. (d) Conditional probability of rupture length unilaterally southeast from the Casa Loma starting point. The fault-geometric estimate of probability of any length bi-lateral rupture is the product of the two unilateral estimates. Section names - SJV: San Jacinto Valley; SJSB: San Jacinto San Bernardino; LY: Lytle Creek; SJC: San Jacinto Stepyer Combined; Anza: San Jacinto Anza; Coyo: SJF Coyote Creek section; Borr: Borrego; SMntn: Superstition Mountain; SHills: Superstition Hills. Other abbreviations given with Figure 7.



601
602
603
604
605
606
607
608
609
610
611
612
613

Figure 9. UCERF3-based rupture length probabilities for rupture starting at the San Jacinto Casa Loma step. (A) Individual annual rupture rates (probabilities) (stars) and incremental magnitude-frequency distribution (solid line, binned at 0.1 magnitude units) of all ruptures in UCERF3 Fault Model 3.1 that end at the Casa Loma step of the San Jacinto fault (west star, **Figure 6**). (B) The corresponding complimentary cumulative distribution (CCD) (solid line) of rupture length for ruptures in (A). Dashed line shows the length CCD if individual rupture probabilities are reduced by the number of subsections (=initiation points) in the rupture. (C) CCD for rupture magnitude for the reduced CCD curve in (B). By this estimate, 54% of single subsection EEW initiations grow to **M** 6.3, 25% become **M** 6.9 to 7.1, and 16% become **M** 7.6 or larger.